Roughness and light scattering of ion-beam-sputtered fluoride coatings for 193 nm

Josep Ferré-Borrull, Angela Duparré, and Etienne Quesnel

Scattering characteristics of multilayer fluoride coatings for 193 nm deposited by ion beam sputtering and the related interfacial roughnesses are investigated. Quarter- and half-wave stacks of MgF_2 and LaF_3 with increasing thickness are deposited onto CaF_2 and fused silica and are systematically characterized. Roughness measurements carried out by atomic force microscopy reveal the evolution of the power spectral densities of the interfaces with coating thickness. Backward-scattering measurements are presented, and the results are compared with theoretical predictions that use different models for the statistical correlation of interfacial roughnesses. © 2000 Optical Society of America

OCIS codes: 310.6860, 290.5820, 180.5810, 140.7240.

1. Introduction

The development of high-quality optical components for applications in the deep-UV–vacuum-UV (DUV–VUV) spectral region has gained considerable interest as a result of the tremendously increasing technological demands of semiconductor and laser material processing industries.[1–3] The achievement of optimized coatings for these components constitutes one of the major challenges, as problems arise that are minor at larger wavelengths.[4,5] Absorption and scattering losses of the layers are critical obstacles that compromise coating performance. Key issues for minimizing these losses consist of a careful selection of the most appropriate coating materials and fine tuning of the deposition processes.

With regard to selection of materials, fluorides are the best candidates for DUV–VUV wavelengths, because they exhibit an electronic bandgap larger than that of oxide materials commonly used for visible and IR applications. However, using fluorides is accompanied by several drawbacks related to the deposition process: Conventional processes such as boat or electron beam require substrate heating for improving adhesion and producing denser films. As a result of the higher thermal expansion coefficient of the fluorides with respect to the substrates, high tensile stress is introduced in the coatings, limiting the total thickness that can be deposited. Furthermore, stress negatively influences the overall quality of the components. In contrast, the ion-beam-sputtering (IBS) technique does not require substrate heating and, moreover, the high energy of the sputtered atoms leads to the deposition of coatings with higher density and compressive stress.[5] It has also been shown that the coatings produced with these techniques are highly homogeneous, whereas the optical constants are close to the bulk values.[2,6] The major problem encountered with ion-beam-sputtered UV coatings is the difficulty of compensating for fluorine deficiencies in the films, which gives rise to optical losses. The feasibility of such coatings with low absorption and a high laser-induced damage threshold has been demonstrated in previous papers.[5,7] Nevertheless, a systematic study of scattering losses at 193 nm and their relation to the film microstructure has not yet been carried out to our knowledge.

The study of scattering losses is closely linked to the characterization of the microstructure of the substrates and coatings. More precisely, the microroughness of the interfaces has proved to be the main source of scattering losses.[8] Consequently, our aim in this paper is to report on investigations of the scattering from ion-beam-sputtered fluoride coatings and its relation to microroughness. The systematic approach used in Ref. 9 for studying coatings for use at 325 nm will be followed. The procedure begins with the definition of a set of sam-

J. Ferré-Borrull and A. Duparré (duparre@iof.fhg.de) are with the Fraunhofer Institute for Applied Optics and Precision Engineering, Schillerstrasse 1, Jena D-07745, Germany. E. Quesnel is with the Laboratoire d'Electronique de Technologie et d'Instrumentation, Département Optronique, Commissariat à l'Energie Atomique, 17 rue des Martyrs, F-38054 Grenoble Cedex 9, France.

Received 3 May 2000; revised manuscript received 31 July 2000.
0003-6935/00/315854-11$15.00/0

Table 1. Designs of the Samples Studied

Optical Thickness (QW)	FS Substrate		CF Substrate	
	QW Designs	HW Designs	QW Designs	HW Designs
1	S–L		S–L, S–H	
2	S–L–H	S–2L	S–L–H	S–2L
3	S–L–H–L		S–L–H–L	
4				S–2L–2H
6	S–$(L–H)^3$	S–2L–2H–2L		S–2L–2H–2L
7	S–$(L–H)^3$–L			
10	S–$(L–H)^5$	S–2L–2H–2L–2H–2L		
20	S–$(L–H)^{10}$		S–$(L–H)^{10}$	S–$(2L–2H)^5$

ples designed specifically to allow for the study of the dependence of the roughness and the scattering on film thickness or number of layers. Then complete characterization of the microroughness of the samples by atomic force microscopy (AFM) and the measurement of the total scattering (TS) at the design wavelength are performed. Finally, the experimental results are analyzed with the help of modeling, which allows for the calculation of roughness-induced elastic scattering using the results of the interfacial roughness characterization as input data. It is important to note that all the TS values presented in this paper (measurements and calculations) correspond to backward scattering. Thus this research is focused on the investigation of scattering at 193 nm while combining the results of different characterization tools. Use of the theory allows us to understand the sources of scattering and can help to establish criteria for optimization of the coatings. For complete knowledge of the losses of ion-beam-sputtered fluoride coatings, further investigations into absorption should be performed.

The paper is organized as follows: In Section 2 the description of the studied samples and the reasons for selection of the substrates and specific film designs are given. Section 3 presents the details of coating deposition and the results obtained by conventional optical characterization. Section 4 provides an overview of the theoretical concepts related to roughness characterization and to the modeling of roughness-induced scattering. In Section 5 the results of the characterization by AFM and of data processing are presented. In Section 6 the results of the TS measurements are discussed and compared with the theoretical predictions. Finally, conclusions are drawn in Section 7.

2. Description of Samples

We investigated samples of two sets of coatings, each with increasing number of layers. CaF_2 (CF) and fused silica (FS) were used as substrates. The designs consist of alternating layers of MgF_2 as low-index (L) and LaF_3 as high-index (H) materials. Several of the designs were composed of quarter-wave (QW) layers, whereas others were stacks of half-wave (HW) layers, each with the design wavelength 193 nm. Table 1 summarizes all samples. The optical thicknesses are given in units of QW's. The designs were chosen with the intention to study the relation of the microroughness and scattering characteristics to thickness or number of layers. HW layer designs were chosen so that their overall thicknesses were the same as those of one of the QW layer designs to compare the microstructural differences between the two kinds of layers.

3. Deposition and Optical Characterization of the Coatings

The films were deposited by sputtering from pure hot-pressed targets with rf ion sources. The load-locked IBS deposition unit is equipped with two cryopumps leading to a base pressure of 4×10^{-8} mbar. The substrates were not intentionally heated so that their temperature remained lower than 60 °C during deposition. The major challenge when depositing sputtered fluoride coatings is to successfully compensate the fluorine deficiency generally observed in the films. That is why such process requires use of reactive deposition conditions by means of introducing supplementary fluorine species during deposition. Initially and for near-UV applications[7] the reactive gas used was CF_4. For the present purpose, diluted fluorine was preferred for limiting the carbon contamination of the films, which can induce undesirable absorption at 193 nm.

As mentioned above, different deposition runs were

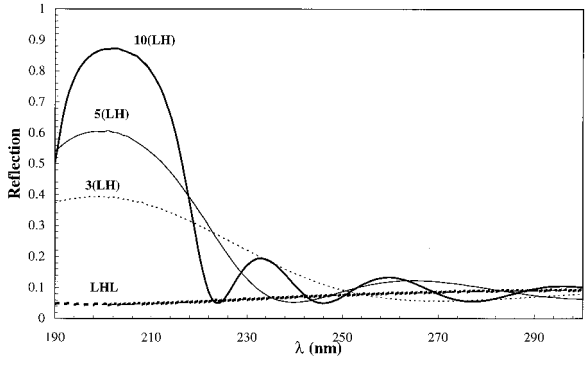

Fig. 1. Reflection spectra for different stacks (first set on FS substrates).

performed corresponding to various QW and HW stacks, with a reference wavelength of 193 nm. The first batch used FS substrates and the second one CF substrates, which were coated in different deposition runs but with the same process parameters. Because of the high stability of the IBS process, no *in situ* quartz or optical monitoring was required. The thickness of each single layer in the stack was controlled only by monitoring of the deposition time. The stack sequence was automatically controlled by sophisticated monitoring software. For the coatings on silica substrates the deposition times were deduced from calibration experiments in which an accurate determination of the thicknesses was obtained from grazing x-ray characterization. In addition, the physical thicknesses of L and H QW layers were deduced from optical design calculations. These optical simulations were performed by use of the real dispersion curves of refractive index n and extinction coefficient k preliminarily measured on 200-nm-thick IBS MgF_2 and LaF_3 single layers. This procedure proved efficient, since the perfect centering of the mirror required only a slight correction of the deposition times between the first and the second set of samples.

Prior to the AFM and the TS analyses the samples were characterized by spectrophotometry from 190 to 800 nm with a Lambda 9 Perkin Elmer spectrophotometer. In fact, two different measurements were made: an initial characterization at wavelengths higher than 200 nm with an integrating sphere for detection that warrants for the reflection a constant measurement error lower than 0.25% and a second measurement between 190 and 250 nm, without an integrating sphere, for maintaining sufficiently high DUV measurement signal. In that case and after adjustment of this second curve to the former one, the measurement of absolute error on R, in the DUV region, can be estimated at ~1%.

Figure 1 illustrates the evolution of the reflective spectral response for different L–H pairs. We note that a slight shift of the centering wavelength (198 nm instead of 193 nm) easily corrected for the CF set.

Table 2. Overview of the Stacks Investigated and Their Reflectance (in percent) at 193 nm

Stack	On Silica Substrates	On CF Substrates
S–L	5	6.2
S–H		12.5
S–L–H	16.8	15.6
S–L–H–L^3	4.6	3.6
S–$(L–H)^3$	38.4	
S–$(L–H)^3$–L	16.1	
S–$(L–H)^5$	57	
S–$(L–H)^{10}$	70	84.9
S–2L	9	
S–2H		7.5
S–2L–2H		7.5
S–2L–2H–2L	8	7.7
S–2L–2H–2L–2H–2L	8	
S–$(2L–2H)^5$		9.2

As a result the CF/$(L–H)^{10}$ design exhibits a better reflection level than the same design on FS (see Table 2). The thicknesses of the QW layers are 33.8 and 28 nm for MgF_2 and LaF_3, respectively. The thickness correction between the two sets of samples corresponds to −0.9 and −0.7 nm per layer for MgF_2 and LaF_3, respectively. This means that, in terms of microstructure, two samples with the same stack design but different substrates can be reasonably compared.

4. Review of Concepts Involving Microroughness Characterization and Theoretical Modeling of Scattering

A. Power Spectral Density Functions and Root-Mean-Square Roughness

Interfacial and surface roughnesses are the main sources of elastic light scattering in thin-film coatings. Consequently, to investigate the origins of scattering in coatings, a complete roughness characterization should be performed. In this section we briefly review the basic theoretical concepts that will be used in the paper with regard to the representation of the roughness properties of a surface.

The microtopography of the samples was measured with an AFM (Digital Instruments, Dimension Model 3000) at different scan sizes and at different positions on each sample. For each measurement the two-dimensional isotropic power spectral density function [PSD(f), with f the spatial frequency] was calculated.[10] This form of the PSD function will be used throughout this study to characterize surface roughness. To combine the results of the different measurements on a given sample, scan sizes were chosen such that the ranges of spatial frequencies of the corresponding PSD functions partially overlap. With this strategy the PSD for different scan sizes can be combined into a single PSD characterizing the surface in the whole range of available spatial frequencies. The value of this combined PSD at a given spatial frequency is the geometrical average of the values of the functions overlapping at that frequency.

Another quantity widely used for roughness characterization is the rms roughness (σ_{rms}). This quantity is useful for direct comparison between two surfaces. It has to be taken into account, however, that the rms roughness of a surface depends on the considered range of spatial frequencies,[11]

$$\sigma_{rms}^2 = 2\pi \int_{f_{min}}^{f_{max}} \mathrm{PSD}(f)\, f\mathrm{d}f, \qquad (1)$$

where f_{min} and f_{max} are the limits of the range of frequencies considered. Consequently, to be able to compare the rms-roughness values of two surfaces, their values must have been obtained by integration within the same range of spatial frequencies.

Since in this paper we wish to obtain the measurement and the modeling of elastic light scattering at 193 nm, the considered range of spatial frequencies is such that the resulting roughness is related to the TS at this wavelength. Light scattered by an isotropic rough surface in a direction given by the polar angle

θ is proportional to the value of the PSD at spatial frequency f. This frequency is related to the angle θ through the grating equation,

$$f = \sin(\theta)/\lambda, \tag{2}$$

where λ is the wavelength. As a result of the geometry of the experimental setup for TS measurement, light scattered into polar angles from 2 to 85 deg is detected. These angular limits define the upper and the lower spatial-frequency limits for the integration of the PSD to yield a rms roughness. The corresponding values for 193 nm are $f_{\min} = 0.181\ \mu\text{m}^{-1}$ and $f_{\max} = 5.162\ \mu\text{m}^{-1}$. The obtained value will be called effective rms roughness ($\sigma_{\text{rms, eff}}$). Effective means that it is the average roughness responsible for scattering at 193 nm. These spatial-frequency limits were chosen to have a figure that allows for mutual comparison of the roughness values of different samples and that is related to their TS. It should be emphasized, however, that there are factors other than the effective rms roughness influencing the TS values. Consequently, the relation between $\sigma_{\text{rms, eff}}$ and TS is not direct.

B. Modeling of Roughness-Induced Scattering in Multilayers

For our calculation of roughness-induced scattering we used the first-order approximation of Bousquet *et al.*[12] The fraction of scattered energy in a given direction per unit of solid angle is the result of the summation

$$\frac{dP}{P_0 d\Omega} = \sum_{i=0}^{p} \sum_{j=0}^{p} C_i C_j^* g_{ij}(\theta), \tag{3}$$

where the indexes i and j count all the interfaces in the coating, p is the number of layers, 0 is the index of the substrate-coating interface, and the asterisk designates complex conjugation. C_i denounce the optical factors that depend on the optical properties of a corresponding ideally smooth coating and on the illumination and observation conditions.[8] $\mathbf{k}$ and $\mathbf{k}_0$ represent the incident and the scattered wave vectors, respectively, with $k = (2\pi/\lambda)\sin(\theta)$, $k_0 = k = (2\pi/\lambda)\sin(\theta_0)$, with θ being the polar angle of scattering and θ_0 the angle of incidence.

The functions g_{ij} represent the roughness statistics of the interfaces in the coating. They are functions of the scattering angle, which is directly related to the spatial frequency through grating equation (2). When $i = j$, g_{ij} corresponds to the PSD of the ith interface. In general, the microroughnesses of buried interfaces (that is, interfaces not accessible by the AFM probe) are not directly measurable, and we must make some assumptions to learn them. Thus, for instance, to determine the PSD of the H–L interface of the sample S–L–H–L, where S is substrate, we assumed that it is the same as the PSD of interface H–air of sample S–L–H, which is indeed directly measurable. It was also assumed that the deposition of further layers on this H–air interface does not modify its statistics. Despite the adoption of these assumptions, there are still buried interfaces where this kind of correspondence cannot be established. For instance, the second H–L interface in the design S–(L–H)^3 (the interface in boldface in S–L–H–L–**H**–**L**–H) has no corresponding sample S–L–H–L–H whose PSD can be directly measured and related to the desired buried interface. For such interfaces the PSD was calculated by means of interpolating the PSD functions of those interfaces that can indeed be measured directly.

For the cases $i \neq j$ the function g_{ij} represents the statistical cross correlation of the roughness of the interfaces i and j. As in the case of the buried interfaces, these cross-correlation functions cannot be directly inferred from AFM measurements. Thus models have to be established that relate the behavior of the g_{ij} with that of the PSD functions of each individual interface. The most widely used models for cross-correlation functions g_{ij} are totally correlated interfaces and totally uncorrelated interfaces.[13] The first one corresponds to the case in which the roughness profile of the substrate is reproduced by all deposited layers. With this model, the same PSD function holds for all interfaces, and all the cross-correlation functions also equal this PSD. The totally uncorrelated interface model is the opposite case: The roughness of an interface is statistically independent of the roughness of any other. With this assumption, the cross-correlation functions g_{ij} ($i \neq j$) vanish, and the PSD of each interface is independent of the others.

These models, however, are based on restrictive assumptions and do not generally apply to real coatings. A more realistic model is that of partially correlated interfaces,[14–16] in which the deposition of each new layer generates a roughness profile $h_i(x, y)$ that reproduces the underlying profile $h_{i-1}(x, y)$ and adds an uncorrelated component $\xi_i(x, y)$:

$$h_i(x, y) = h_{i-1}(x, y) + \xi_i(x, y). \tag{4}$$

This leads to a relation between the PSD functions of each interface and the cross-correlation functions g_{ij} of the form

$$g_{ij} = g_{ii}, \qquad \text{where } i = \text{minimum}(i, j). \tag{5}$$

Although the partially correlated interface model is the most likely model to match the actual characteristics of our coatings, results for the other two models will also be obtained and compared with the scattering measurements, since this comparison is a way of verifying the hypothesis used in the calculations.

For calculating TS, expression (3) has to be integrated over the desired scattering hemisphere (backward or forward scattering). Since the incident beam is unpolarized and all polarization directions of the scattered light are detected, this expression has to be evaluated for all four possible combinations of the polarization of incident beam and detected light. Then the results are added to yield the total scattered

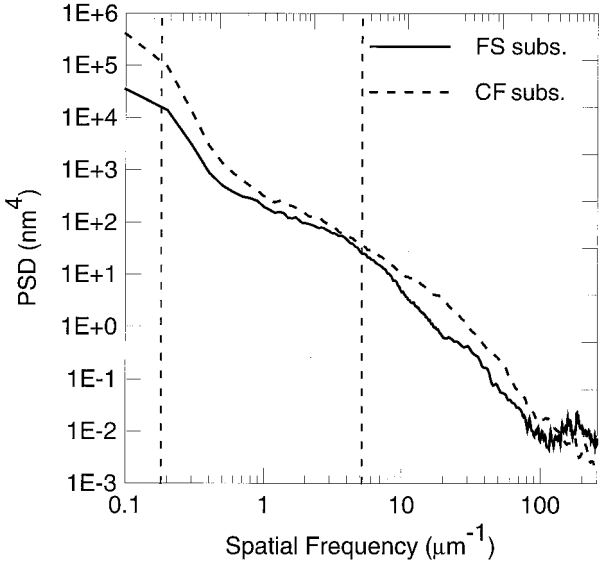

Fig. 2. PSD functions of the substrates used in the experiments.

flux in a given direction. Finally, the value of the TS is the result of the integral

$$\mathrm{TS} = \int_{\theta_{\min}}^{\theta_{\max}} \int_{0}^{2\pi} \frac{\mathrm{d}P}{P_0 \mathrm{d}\Omega}, \tag{6}$$

where $\theta_{\min}$ and $\theta_{\max}$ correspond to the range of angles in which the scattered light is collected.

5. Roughness Characterization

Prior to the roughness characterization of the IBS fluoride coatings it is important to determine the roughness of the substrates used in the experiments. First, substrate roughness constitutes a component of the overall roughness of the coating, and, second, it may also influence film growth. Figure 2 displays the PSD functions of the substrates. The vertical lines in the graphs are placed at the frequency limits defined by scattering angles 2 and 85 deg at 193 nm. Both substrates reveal similar characteristics, with the CF surfaces being slightly rougher. The results also reveal that the PSD functions of both types of substrates approximately build a straight line, which is in agreement with expected statistics for polished surfaces.[17] Table 3 contains the rms roughnesses obtained from AFM measurements at different scales and the resulting $\sigma_{\mathrm{rms,\,eff}}$ calculated by application of expression (1) to the PSD functions.

The structural properties of the coatings are qualitatively evaluated through observation of top-view images of AFM measurements. A selection of these measurements is presented in the following figures. Figure 3 corresponds to the sample with a MgF_2 QW single layer on FS. The image taken at a smaller scan size reveals granular structures that correspond to the tops of the characteristic columnar structures of fluoride coatings. Their lateral size was estimated between 6 and 7 nm for both the MgF_2 and the LaF_3 coatings. The measurement for the HW layer

Table 3. Roughness Values of the Substrates Used in the Experiments

	Rms Roughness from AFM Measurements (nm)		
Substrate	1 μm × 1 μm Scan	10 μm × 10 μm Scan	$\sigma_{\mathrm{rms,\,eff}}$
FS	0.12	0.12	0.09
CF	0.17	0.24	0.14

of MgF_2 onto FS shows that both the roughness and the lateral size of the structures increase compared with the QW layer coating. This increment in the size of the lateral structures can be explained because, throughout the layer thickness, the columns are not strictly rectangular and can be more or less conical.[18]

A remarkable effect observed in the multilayer coatings is that several samples exhibited a tendency of the columnar structures to aggregate and form superstructures with a diameter of ~300 nm. This tendency was observed especially with samples in which a low-index layer was deposited onto an already existing high-index layer but also for the 2H and the 2L–2H coatings onto CF. Figure 4 contains an example of this effect corresponding to the sample with design L–H–L deposited onto CF. A previous study[18] showed that the IBS MgF_2 coatings exhibit a regular growth that cannot explain the formation of such aggregations. Nevertheless, in a current study (to be published) on IBS LaF_3 films, TEM cross sections indicate the presence of large grains in the films. We believe the growth of the LaF_3 films to be at the origin of these aggregations.

Figure 5 allows us to compare the growths of the QW and the HW layers. It shows the AFM top-view image for the coating S–2L–2H–2L on FS. Note that the height scale in these images is higher than in Fig. 4, since the aggregates are slightly higher compared with the QW design. The size of the granular structures is larger than in the QW layer coating, as also observed for the single-layer case.

Table 4 summarizes the rms roughnesses obtained from the measurements at different scan sizes along with the resulting effective rms roughnesses ($\sigma_{\mathrm{rms,\,eff}}$). As expected, the measurements show a gradual increase in roughness with increasing num-

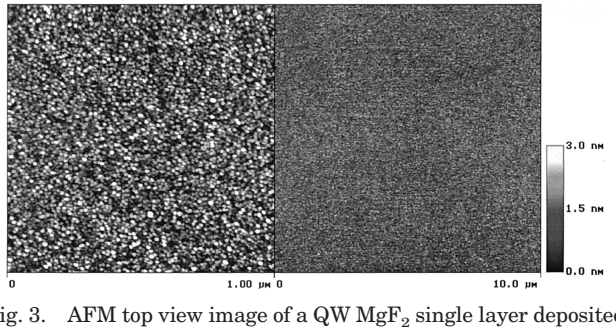

Fig. 3. AFM top view image of a QW MgF_2 single layer deposited on FS.

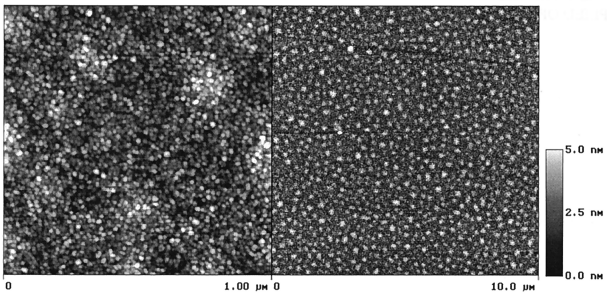

Fig. 4. AFM top view image of L–H–L design deposited on CF.

ber of layers (or equivalently, with increasing overall thickness of the coating). A dramatic increase of the effective roughness can be observed for the samples containing the aggregations discussed above. Comparison of these values with the roughnesses of coatings produced by conventional evaporation techniques proves that the IBS technique results in fluoride coatings with much smaller roughness.[4] This result can be expected on the basis of the mechanical and structural properties exhibited by IBS fluoride coatings (high packing density, low inhomogeneity, compressive stress).[2,5]

The PSD functions sustain these observations and

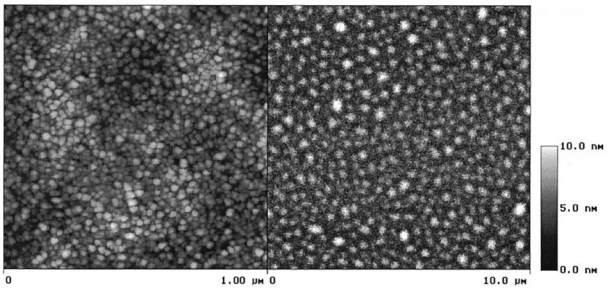

Fig. 5. AFM top view image of a 2L–2H–2L coating deposited on FS.

complement the information on the microstructure of the IBS coatings. Figure 6 displays a selection of PSD functions for QW stacks. Graph (a) corresponds to the samples with FS substrate, and (b) contains the data for the same designs deposited on CaF_2. The PSD functions of the substrates are included as reference. Comparison of the two graphs reveals that the PSD of a given design is similar for both substrates. This indicates that the film growth is not influenced by the type of substrate. It is interesting to note that the deposition of the high-index layer of the system S–L–H adds a small roughness component to the sample. In contrast, the deposition of the next L layer on this H layer induces the formation of aggregations that are clearly obvious as a local maximum near the 3-μm^{-1} spatial frequency.

This spatial frequency is included in the range of spatial frequencies inducing TS at 193 nm. Consequently, this local maximum is responsible for the remarkable increase in $\sigma_{rms,\,eff}$ observed for these samples. Furthermore, the height of the maximum does not vary noticeably with increasing number of layers, meaning that the aggregates do not increase in height. Since the intrinsic roughness of the coating does increase with the number of layers, for samples with large numbers of layers, the contribution of the aggregates to the overall roughness is small compared with the contribution from the intrinsic roughness of the coating. This is shown, for example, in the AFM image of Fig. 7, displaying sample $(L–H)^{10}$ on FS. The aggregations are still visible in the picture but with a small contrast. The corresponding maximum, however, is not obvious from the PSD curve.

For the sake of completeness the PSD functions of a representative selection of the HW coatings are presented in Fig. 8. The development of the roughness is similar to the QW designs with the single exception that the coating 2L–2H on CF exhibits aggregations.

Table 4. Roughness Values of the Produced Coatings

	Rms Roughness from AFM Measurements (nm)					
	FS Substrate			CF Substrate		
Design	1 μm × 1 μm	10 μm × 10 μm	$\sigma_{rms,\,eff}$	1 μm × 1 μm	10 μm × 10 μm	$\sigma_{rms,\,eff}$
S–L	0.43	0.23	0.11	0.44	0.32	0.12
S–H				0.47	0.41	0.19
S–L–H	0.48	0.31	0.12	0.48	0.37	0.14
S–L–H–L	0.84	0.74	0.47	0.89	0.97	0.56
$S–(L–H)^3$	1.10	0.98	0.53			
$S–(L–H)^3–L$	1.21	1.27	0.57			
$S–(L–H)^5$	1.36	1.20	0.52			
$S–(L–H)^{10}$	1.90	1.82	0.76	1.63	1.77	0.68
S–2L	0.66	0.46	0.14			
S–2H				0.58	0.58	0.51
S–2L–2H				0.85	0.71	0.36
S–2L–2H–2L	1.34	1.59	1.20	1.06	0.89	0.31
S–2L–2H–2L–2H–2L	1.57	1.46	0.96			
$S–(2L–2H)^5$				1.91	1.82	0.61

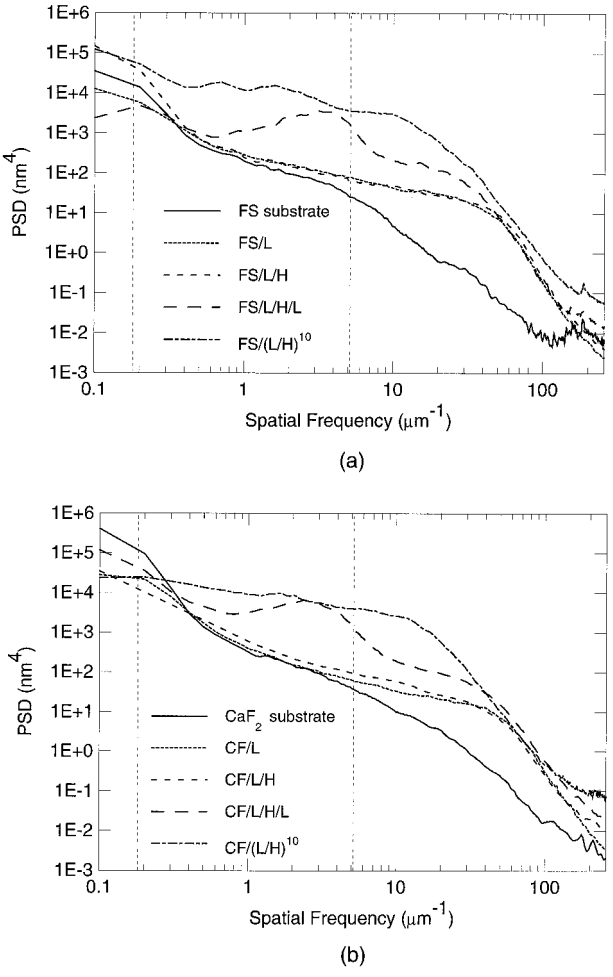

Fig. 6. Selected PSD functions for the samples with QW designs.

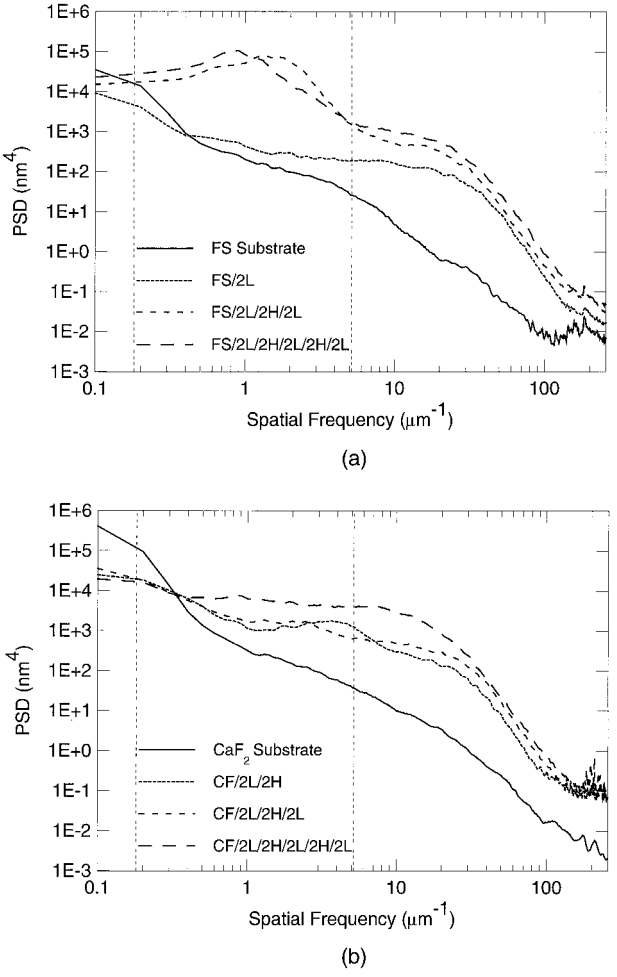

Fig. 8. Selected PSD functions for samples with HW designs.

The PSD functions presented in this section have been used as input data for calculating the expected scattering. Another input needed for the scattering modeling is the model of correlation between the roughness statistics of the interfaces. This information can be obtained from the graphs of Figs. 6 and 8: the PSD's of the single-layer coatings reproduce the PSD of the substrate in the low- and the high-spatial-frequency ranges and exhibit a component associated with the intrinsic roughness of the layers in the central-spatial-frequency region. As more layers are deposited, this intrinsic roughness increases until the influence of the substrate is lost within the whole range of spatial frequencies. This observation suggests that the roughnesses of the interfaces follow a partially correlated (additive) model.

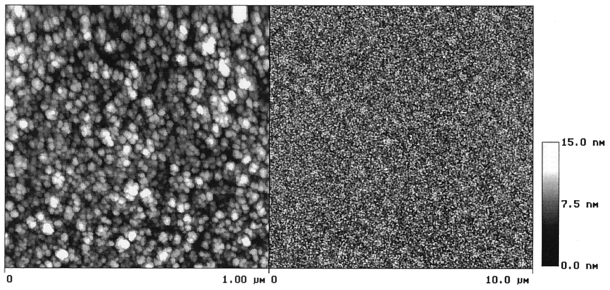

Fig. 7. AFM top view image of the (L–H)^{10} sample deposited on FS.

6. Measurement and Modeling of Total Scattering

For all samples discussed in Sections 1–5 TS was measured at 193 nm and was compared with results obtained from model calculations accomplished with the roughness data obtained by AFM and application of different models for the cross correlation of the interfacial roughness statistics.

The TS measurements were performed with a setup developed at the Fraunhofer Institute, which is capable of measuring backward and forward scatter at several wavelengths ranging from the UV to the IR spectral region (see Fig. 9).[19,20] The setup follows the instructions given in the European standard ISO/DIS 13696.[21] This standard draft has been successfully tested for visible wavelengths through a recent international round-robin experiment performed at 633 nm.[22] For wavelengths below 200 nm, however, future intensive studies into the specific requirements, problems, and effects occurring in

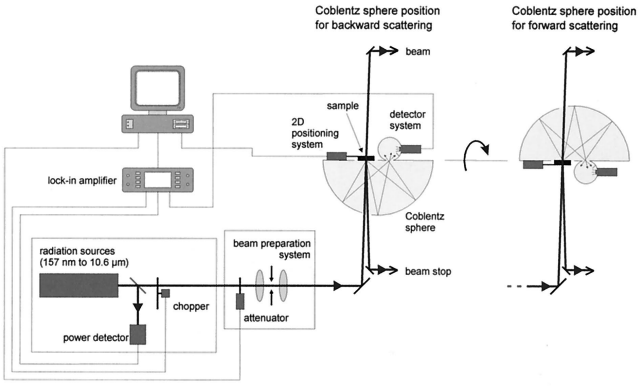

Fig. 9. Diagram of setup for TS measurement. For the measurements in this study backscatter configuration was used. A similar setup for measurements at 157 nm is placed in a vacuum chamber and uses excimer laser or deuterium lamp radiation. 2D, two dimensional.

the DUV–VUV spectral region, will reveal how and to what extent the ISO/DIS standard[21] has to be modified. The setup is operated down to 193 nm in air with a deuterium lamp. An excimer laser can be used alternatively. For measurements at 157 nm we developed a special setup with the same basic components but placed in a steel chamber allowing for operation in both vacuum and nitrogen atmospheres. Excimer laser radiation or a deuterium lamp is used as a light source.[23]

For the measurements described in this paper the wavelength of 193 nm was filtered out from the radiation of the deuterium lamp by means of a set of dielectric mirrors. The beam was modulated by a chopper and then spatially filtered and collimated to optimize beam quality. The light was directed onto the sample at nearly normal incidence and the specular reflected beam guided back through the aperture of the Coblentz sphere. The Coblentz sphere imaged the backward-scattered light in the range of polar angles between 2 and 85 deg onto the detector system. A positioning device allowed for automatic scanning of the sample, thus providing one- or two-dimensional scatter diagrams. The measurements in this study were performed along two perpendicular lines, and the obtained data were condensed into a single value with the data-reduction procedure included in standard ISO/DIS 13696.[21]

The calibration of the setup was accomplished by means of registering the signal produced by a standard Lambertian diffuser. The background level of the system (signal measured without sample) was between 2×10^{-5} and 5×10^{-5}. However, the minimum measurable value of the setup was limited by the quality of the incident beam. The reason for this is that, to optimize the light flux on the sample, the incident beam is not completely parallel but slightly divergent, and, as a consequence, a small part of the reflected beam can be coupled into the Coblentz sphere and accounted for as scattered light. When we measure transparent samples, as is the case in the present study, the beam is reflected at the front and the back surfaces of the sample, and thus the minimum measurable TS, will depend on the reflectances of both surfaces.

To estimate the fraction of reflected beam energy coupled into the sphere, the signal produced by a superpolished silicon wafer was measured and was translated into an equivalent value of scattering by means of the calibration signal.[24] Since the expected scattering is two orders of magnitude smaller than the measured scattering (S_{Si}), it has to be concluded that this measured value corresponds to the fraction of the reflected beam that remains inside the sphere. Using S_{Si} allows us to estimate the amount of reflected beam light recorded as scattering,

$$S_{\mathrm{Beam}} = \frac{S_{\mathrm{Si}}}{R_{\mathrm{Si}}}\left[R_1 + R_2\frac{(1-R_1)^2}{1-R_1R_2}\right], \tag{7}$$

where R_1 and R_2 are the reflectances for the front and the back surfaces of the sample, respectively. R_{Si} is the reflectance of silicon. In the derivation of this last expression, multiple reflections in the substrate were taken into consideration. S_{Beam} will be referred to as the sensitivity of the setup, since it is the most limiting factor. It should be emphasized, however, that this value does not strictly represent the sensitivity but the minimum measurable scattering.

The modeling of scattering provides information about which samples can actually be measured with the setup. Thus Table 5 shows the sensitivities for all samples with QW stacks obtained from the calibration data. Together with these values we present the expected TS calculated from the optical and the roughness characterizations. TS was modeled for a different correlation hypothesis: the partially correlated interface model, the uncorrelated model, and finally a modification of the fully correlated interface model that will be called top-down correlated interfaces. In the latter model the PSD of the coating–air interface was used for all interfaces and their cross correlations. Neither of the two lastly considered models is likely to match entirely the real correlation properties of the interfaces in the coating. Nevertheless, they are reasonable because their results represent the extreme values of scattering that can be expected from a sample. This table reveals that TS measurements on the samples with a larger number of layer pairs are likely to be less sensitive to errors.

The measured TS of all samples examined in this study are summarized in Table 6. The scattering of the bare substrate was also measured and included in the table for reference. Obviously, TS is systematically higher for coatings on FS as compared with coatings on CF. This holds even for those samples with a small number of layers, for which the effective roughness of the coatings on CF is higher than for coatings on FS. This effect is particularly noticeable in the case of bare substrates for which the TS is different, whereas the substrates have similar rms roughnesses and refractive indices. Furthermore,

Table 5. Minimum Measurable Values of TS (Sensitivity) for the Samples with QW Designs

Sample	Sensitivity	Calculated TS, Partially Correlated	Calculated TS, Uncorrelated	Calculated TS, Top-Down Correlated
FS–L	2.75×10^{-5}	3.65×10^{-6}	4.34×10^{-6}	3.26×10^{-6}
FS–L–H	7.62×10^{-5}	8.43×10^{-6}	5.01×10^{-6}	1.08×10^{-5}
FS–L–H–L	2.09×10^{-5}	6.74×10^{-5}	7.30×10^{-5}	1.03×10^{-5}
FS–(L–H)^3	1.82×10^{-4}	1.84×10^{-4}	7.08×10^{-5}	4.97×10^{-4}
FS–(L–H)^3–L	8.20×10^{-5}	9.18×10^{-5}	3.72×10^{-4}	2.78×10^{-4}
FS–(L–H)^5	2.88×10^{-4}	5.32×10^{-4}	1.42×10^{-4}	7.85×10^{-4}
FS–(L–H)^{10}	4.04×10^{-4}	1.37×10^{-3}	3.11×10^{-4}	2.17×10^{-3}
CF–L	4.77×10^{-5}	8.66×10^{-6}	7.47×10^{-6}	6.45×10^{-6}
CF–H	2.79×10^{-5}	6.78×10^{-6}	1.32×10^{-5}	2.10×10^{-5}
CF–L–H	7.88×10^{-5}	1.26×10^{-5}	8.40×10^{-6}	1.46×10^{-5}
CF–L–H–L	1.94×10^{-5}	9.36×10^{-5}	1.02×10^{-4}	1.11×10^{-5}
CF–(L–H)^{10}	4.43×10^{-4}	1.37×10^{-3}	2.80×10^{-4}	1.61×10^{-3}

Note: comparison of these values with the expected TS calculated under different correlation assumptions reveals which samples can actually be measured.

the TS of the coatings on FS was found to be between two and five times higher than the sensitivity of the setup, whereas for the coated CF it is of the same order of magnitude. All this leads to the conclusion that the FS substrates used in the experiments additionally contribute to scattering at 193 nm. This additional contribution could even be the result of inelastic scattering such as fluorescence induced in the bulk of the FS.

When we compare the values in Table 6 with the scattering levels of samples with the same design and deposited onto substrates with similar characteristics but with conventional evaporation techniques,[4] two different tendencies are observed depending on the number of layers. For the coatings with designs S–L, S–H, S–L–H, and S–L–H–L, the scattering of the IBS samples is smaller than that of samples produced by evaporation. For larger number of layers (designs S–(L–H)^5 and S–(L–H)^{10}] the values obtained by all deposition techniques are similar with a tendency of IBS coatings yielding lower scatter values.

Figure 10 shows the measured TS together with the results of calculation that use the theoretical model presented above for those samples whose expected scattering is higher than the sensitivity of the measurement. Analyzing the graphs, we can conclude that the values calculated from the partially correlated interface model are smaller than the measured scatter, whereas those obtained from the top-down correlated interface model are closer to the measured TS. The first observation can be explained by underestimation of the PSD function of the buried interfaces, thus resulting in excessively small scattering values. In the case of calculations with the top-down correlated interface model the effect is the opposite: The PSD functions of the buried interfaces are surely overestimated, and thus the calculated scattering is larger than the value obtained by the partially correlated model [except for the coating (L–H)^3–L on FS where the interference of the scattering from the different interfaces is destructive and thus the effect inverted). We believe that the better agreement of the experimental results with the top-down correlated interfaces hypothesis is a consequence of compensating the PSD overestimation of the buried interfaces by damping of the electrical field in the inner layers of the coatings.

This agreement demonstrates that, for multilayer

Table 6. Measured Values of Total Scattering at 193 nm

Design	FS Substrate	CF Substrate
S	4.59×10^{-4}	1.06×10^{-4}
S–L	6.80×10^{-4}	2.52×10^{-4}
S–H		4.67×10^{-4}
S–L–H	5.57×10^{-4}	2.13×10^{-4}
S–L–H–L	6.06×10^{-4}	3.26×10^{-4}
S–(L–H)^3	7.26×10^{-4}	
S–(L–H)^3–L	6.01×10^{-4}	
S–(L–H)^5	8.91×10^{-4}	
S–(L–H)^{10}	1.86×10^{-3}	1.19×10^{-3}
S–2L	5.75×10^{-4}	
S–2H		3.59×10^{-4}
S–2L–2H		2.13×10^{-4}
S–2L–2H–2L	6.53×10^{-4}	2.45×10^{-4}
S–2L–2H–2L–2H–2L	5.57×10^{-4}	
S–(2L–2H)^5		6.08×10^{-4}

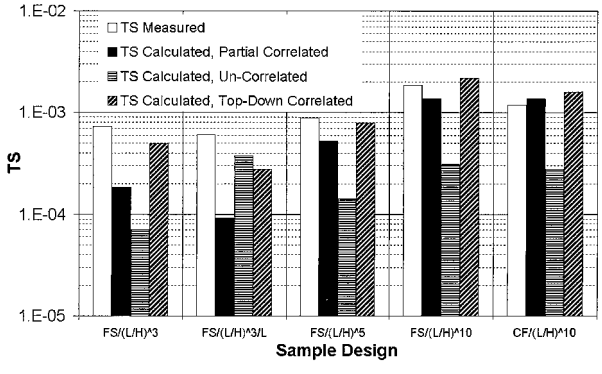

Fig. 10. Comparison of measured and calculated TS for samples with expected scattering higher than the sensitivity of the measurement setup.

fluoride coatings, interfacial roughnesses constitute the main source of scattering losses and that the scattering can be predicted from microroughness characterization as long as an appropriate model for the development of the roughness in the buried interfaces is adopted.

7. Conclusions

In this study manufacturing and systematic characterization of the microroughness and total scattering (TS) properties of fluoride multilayer coatings for the deep-UV (DUV) range (193 nm) with an ion-beam-sputtering (IBS) deposition technique has been accomplished. UV-grade fused silica (FS) and CaF_2 (CF) were used as substrates, and MgF_2 and LaF_3 were used as low- (L) and high-index (H) materials, respectively.

Microroughness characterization was carried out by highly sensitive AFM measurements at two different scan sizes, and the surface roughness statistics were described by use of power spectral densities (PSD's) as well as the rms roughness effective for scattering at 193 nm. The scattering characterization was performed by means of measuring TS in the backward direction and comparing the results with the calculation of the expected scattering. We accomplished the calculations by using a convenient theoretical model and employing the data from microroughness characterization. Modeling of scattering included different assumptions on the statistical correlation between the roughnesses of the coating interfaces.

Microroughness characterization enabled the observation of the development of the roughness in samples with increasing number of consecutive L and H layers. Examination of the PSD functions proved that the development of the roughness was in good agreement with the partially correlated interface model. AFM measurements also demonstrated that the lateral size of the columnar structures increased with increasing total coating thickness. This leads to the conclusion that the deposition of each new layer does not cut off the columnar growth. Another effect observed is the aggregation of columnar structures into superstructures for coatings with three or more layers as well as for the coatings with designs 2H and 2L–2H deposited on CF. This effect might be related to the observed presence of large grains in the volume of LaF_3 films produced by IBS. These aggregations induce a significant increase in the rms roughness, since their characteristic size corresponds to spatial frequencies included in the range of frequencies related to TS at 193 nm.

Comparison of the roughnesses of the samples studied in this paper with roughnesses of similar samples (this is, with the same design and materials deposited onto substrates of the same refractive index and surface roughness) with conventional evaporation techniques shows that the IBS technique produces smoother coatings, even in the case of the formation of aggregations.

Total backscattering measurements revealed that for the samples with small numbers of layers the scattering induced by the coating was smaller than the scattering level of the substrate (in the case of samples with FS substrates) or was of the same order of magnitude as the sensitivity of the measurement system. However, the measured scattering for the samples deposited by IBS was always smaller than the scattering of similar samples obtained with conventional evaporation techniques. It was also shown that for samples with large numbers of layers the scattering level of the coating was the main source of losses. Comparison with conventionally deposited coatings reveals that IBS tended to lead to the smallest scatter.

Calculations of the expected scattering from microroughness characterization confirm the conclusions presented in the preceding paragraph. The calculated values for samples with small optical thicknesses are much smaller than the measured scatter. This indicates the presence of contributions to the measured TS in addition to those induced by interface roughness. However, calculations and measurements reveal better agreement for samples with high numbers of layers. In this case best modeling is achieved by the top-down correlated interfaces. This is in contrast to the idea that the partially correlated interface model is more adequate for representing the roughness correlation of the interfaces. These results also lead to the conclusion that the PSD functions of the buried interfaces are underestimated when the partially correlated model is used.

The authors thank Jörg Steinert and Stefan Gliech for their support with the measurements and for fruitful discussions and Aurélien Petit dit Dariel for his contribution to the deposition of fluoride coatings. The authors also gratefully acknowledge the support of the European Commission [Training, Mobility, and Research (TMR) network "High-quality UV-coatings," contract ERBFMRX-CT97-0101].

References

1. U. Stamm, R. Paetzel, I. Bragin, J. Kleinschmidt, D. Basting, and F. Voss, "Recent developments in industrial excimer laser technology," in *XI International Symposium on Gas Flow and Chemical Lasers and High-Power Laser Conference*, D. R. Hall and H. J. Baker, eds., Proc. SPIE **3092,** 485–492 (1997).
2. D. Ristau, W. Arens, S. Bosch, A. Duparré, E. Masetti, D. Jacob, G. Kiriakidis, F. Peiró, E. Quesnel, and A. V. Tikhonravov, "UV-Optical and microstructural Properties of MgF_2 coatings deposited by IBS and PVD processes," in *Advances in Optical Interference Coatings*, C. Amra and H. Macleod, eds., Proc. SPIE **3738,** 436–445 (1999).
3. A. Duparré, R. Thielsch, N. Kaiser, S. Jakobs, K. Mann, and E. Eva, "Surface finish and optical quality of CaF_2 for UV-litography applications," in *Optical Microlithography XI*, L. Van den Hove ed., Proc. SPIE **3334,** 1048–1054 (1998).
4. W. Arens, D. Ristau, J. Ullmann, C. Zaczek, R. Thielsch, N. Kaiser, A. Duparré, O. Apel, K. Mann, H. Lauth, H. Bernitzki, J. Ebert, S. Schippel, and H. Heyer, "Properties of fluoride DUV-excimer laser optics: influence of the number of dielectric layers," in *Laser-Induced Damage in Optical Materials: 1999*, G. J. Exarhos, A. H. Guenther, M. R. Kozlowski, K. L. Lewis, and M. J. Soileau, eds., Proc. SPIE **3902,** 250–259 (2000).

5. J. Dijon, E. Quesnel, B. Rolland, P. Garrec, C. Pellé, and J. Hue, "High damage threshold fluoride UV mirrors made by ion beam sputtering," in *Laser-Induced Damage in Optical Materials Symposium, Boulder, 1997*, Proc. SPIE **3244,** 406–416 (1998).
6. E. Quesnel, A. Petit dit Dariel, A. Duparré, J. Ferré-Borrull, and J. Steinert, "DUV light scattering and morphology of ion beam sputtered fluoride coatings," in *Advances in Optical Interference Coatings*, C. Amra and H. Macleod, eds., Proc. SPIE **3738,** 410–416 (1999).
7. E. Quesnel, M. Berger, J. Cigna, D. Duca, C. Pellé, and F. Pierre, "Near-UV to IR optical characterization of YF_3 thin films deposited by evaporation and ion beam processes," in *Developments in Optical Component Coatings*, I. Reid, ed., Proc. SPIE **2776,** 366–372 (1996).
8. A. Duparré, "Light scattering of thin dielectric films," in *Thin films for Optical Coatings*, R. E. Hummel and K. H. Günter, eds., Vol. 1 of Handbook of Optical Properties Series (CRC, Boca Raton, Fla., 1995), pp. 273–304.
9. S. Jakobs, A. Duparré, and H. Truckenbrodt, "Interfacial roughness and related scatter in ultraviolet optical coatings: a systematic experimental approach," Appl. Opt. **37,** 1180–1193 (1998).
10. C. Ruppe and A. Duparré, "Roughness analysis of optical films and substrates by atomic force microscopy," Thin Solid Films **288,** 8–13 (1996).
11. J. M. Bennett and L. Mattsson, *Introduction to Surface Roughness and Scattering*, 2nd ed. (Optical Society of America, Washington, D.C., 1999).
12. P. Bousquet, F. Flory, and P. Roche, "Scattering from multilayer thin films: theory and experiment," J. Opt. Soc. Am. **71,** 1115–1123 (1981).
13. J. M. Elson, J. P. Rahn, and J. M. Bennett, "Light scattering from multilayer optics: comparison of theory and experiment," Appl. Opt. **19,** 669–679 (1980).
14. C. Amra, "Light scattering from multilayer optics. 1. Tools of investigation," J. Opt. Soc. Am. A **11,** 197–210 (1994).
15. C. Amra, "Light scattering from multilayer optics. 2. Application to experiment," J. Opt. Soc. Am. A **11,** 211–226 (1994).
16. A. Duparré and H.-G. Walther, "Surface smoothing and roughening by dielectric thin film deposition," Appl. Opt. **27,** 1393–1395 (1988).
17. E. L. Church, "Fractal surface finish," Appl. Opt. **27,** 1518–1526 (1988).
18. D. Jacob, F. Peiró, E. Quesnel, and D. Ristau, "Microstructure and composition of MgF_2 optical coatings grown on Si substrate by PVD and IBS processes," Thin Solid Films **360,** 133–138 (2000).
19. A. Duparré and S. Gliech, "Quality assessment from supersmooth to rough surfaces by multiple-wavelength light scattering measurement," in *Scattering and Surface Roughness*, Z. Gu and A. A. Maradudin, eds., Proc. SPIE **3141,** 57–64 (1997).
20. A. Duparré and G. Notni, "Multi-type surface and thin film characterization using light scattering, scanning force microscopy and white light interferometry," in *Optical Metrology*, G. A. Al-Jumaily ed., SPIE Vol. CR 72 of SPIE Critical Review Papers Series (Society of Photo-Optical Instrumentation Engineers, Bellingham, Wash., 1999), pp. 213–231.
21. International Organization for Standardization, Working Group 6, Subcommittee 9, Technical Committee 172, "Optics and optical instruments—test methods for radiation scattered by optical components," ISO/DIS 13696 (International Organization for Standardization, Geneva, 1999).
22. P. Kadkhoda, A. Müller, D. Ristau, A. Duparré, S. Gliech, H. Lauth, U. Schuhmann, N. Reng, M. Tilsch, R. Schuhmann, C. Amra, C. Deumie, C. Jolie, H. Kessler, T. Lindström, C. G. Ribbing, and J. M. Bennett, "International round-robin experiment to test the International Organization for Standardization total scattering draft standard," Appl. Opt. **39,** 3321–3332 (2000).
23. S. Gliech, J. Steinert, A. Duparré, "VUV light scattering measurement of optical components for lithography applications," in *Optical Metrology Roadmap for the Semiconductor, Optical, and Data Storage Industries*, G. A. Al-Jumaily, A. Dupparé, and B. Singh, eds., Proc. SPIE **4099,** 213–231 (2000).
24. S. Gliech, "Total light scattering measurement from the VUV to IR spectral region," Ph.D. dissertation (University of Ilmenau, Ilmenau, Germany) (in preparation).